Remnant X-ray Magnetic Circular Dichroism Investigation of the Local Magnetic Contributions to the Magnetization of a Coercive Bimetallic Molecule-Based Magnet

Cyrille Train,[†] François Baudelet,[‡] and Christophe Cartier dit Moulin*[,†,‡]

Laboratoire de Chimie Inorganique et Matériaux Moléculaires, UMR 7071, Université Pierre et Marie Curie (UPMC), 4 Place Jussieu, Case 42, 75252 Paris Cedex 05, France, and Laboratoire pour l'Utilisation du Rayonnement Electromagnétique, Bât. 209D, Université Paris-Sud, BP 34, 91 898 Orsay Cedex, France

Received: February 3, 2004; In Final Form: May 19, 2004

X-ray magnetic circular dichroism (XMCD) measurements have been performed at the Cr and Fe K-edges for the two-dimensional oxalate-based magnet $\{[N(C_4H_9)_4][Fe^{II}Fe^{III}_{0.77}Cr^{III}_{0.23}(ox)_3]\}_n$ (ox = $C_2O_4^{2-}$) in its long-range ordered magnetic state. First, the XMCD spectra recorded under a 2 T applied magnetic field are used to probe the local exchange interaction between the metal ions through the relative orientation of their spins in the magnetic field. The remnant local magnetic moments on the Cr and Fe ions have been clearly evidenced, analyzed, and compared to the total remnant magnetization measured by conventional magnetometry. The respective impact of single ion anisotropy, magneto-structural anisotropy, and exchange interaction on the remnant magnetic state is then discussed.

Introduction

The flexibility of coordination chemistry allows us to synthesize, following a rational way, new objects with original and controlled magnetic properties.[1,2] In this research field, high spin molecules such as $Mn_{12}O_{12}(O_2CCH_3)_{16}(H_2O)_4\cdot 4H_2O\cdot 2CH_3CO_2H$ (Mn_{12}-ac) show peculiar magnetic properties.[3,4] This so-called single molecule magnet presents a remnant magnetization and a spin tunneling effect below 2 K.[4,5] The origin of these properties is generally attributed to the anisotropy of the paramagnetic ions and/or the magneto-structural anisotropy of the compound.

X-ray magnetic circular dichroism (XMCD) measures the difference in absorption between right and left circularly polarized X-rays. It joins the local selectivity of X-ray absorption spectroscopy to magnetic measurements. It thus probes selectively the magnetic contributions of each element to the macroscopic magnetic properties of a material.[6−8] Moreover, at the $L_{2,3}$-edges, XMCD allows us to separate the spin and orbital contributions to the magnetic moment,[9] for example, to have access to the magnetic anisotropy of each spin carrier. For Mn_{12}-ac, recent XMCD measurements under magnetic field combined with crystal-field multiplet calculations have shown that the orbital contributions to the magnetic moments of the Mn(III) and Mn(IV) ions were surprisingly small for both ions.[10]

Our ultimate goal is to record the remnant XMCD signals for single molecule magnets without magnetic field after saturation of the sample. Up to now, nearly all XMCD signals were recorded while applying a high magnetic field in order to saturate the sample and therefore increase the intensity of the XMCD signals. Rare were the XMCD experiments performed in the remnant state. Such experiments are crucial to determine the spin and orbital magnetic moments in zero field. They allow us to weigh the respective impact of single ion anisotropy, magneto-structural anisotropy, and exchange interaction on the remnant magnetic state. Such a work is attractive but necessitates the recording of XMCD signals at very low temperature (below 1.5 K),[11] which is experimentally difficult to realize. A ^{3}He−^{4}He dilution refrigerator experimental apparatus was actually especially developed for such measurements.[12]

The work presented here has to be considered as the first necessary step in the study of single molecule magnets at very low temperature. We have to demonstrate the feasibility of recording good quality remnant XMCD signals at reachable temperatures and to correlate the local remnant magnetization of each element to the macroscopic magnetic properties. Remnant local magnetic moments on Cr and Ni ions have been previously evidenced by XMCD for the two-dimensional oxalate-based magnet $\{[N(C_4H_9)_4][NiCr(ox)_3]\}$ (ox = $C_2O_4^{2-}$).[13] Unfortunately, the lowest temperature reachable with the experimental setup (11 K) was too close to the Curie temperature of the compound (T_C = 16 K) to establish a convincing correlation between the XMCD signals and the macroscopic remnant magnetization. We present here new XMCD measurements performed on another two-dimensional oxalate-based magnet, $\{[N(C_4H_9)_4][Fe^{II}Fe^{III}_{0.77}Cr^{III}_{0.23}(ox)_3]\}$. Compared to the case of the NiCr analogue, the proper choice of the chromium contents in the $\{[N(C_4H_9)_4][Fe^{II}Fe^{III}_xCr^{III}_{1-x}(ox)_3]\}$ solid solution leads to compounds with both higher T_C's for $x \geq 0.5$[14] and higher coercive forces for $0.5 \leq x \leq 0.8$.[15] So, we expect to obtain for this compound good quality remnant XMCD signals to be safely compared to the remnant macroscopic properties of the material. With such local magnetic measurements, we shall see if the contribution of the Fe and Cr ions to the macroscopic remnant magnetization depends on the intrinsic anisotropy of the ion, which is expected to be higher for the high spin Fe(II) ions than for the Cr(III) ones because of orbital degeneracy in the former case.[16]

Experimental Section

The studied material, $\{[N(C_4H_9)_4][Fe^{II}Fe^{III}_{0.77}Cr^{III}_{0.23}(ox)_3]\}$, is a member of the well-studied family of two-dimensional

* To whom correspondence should be addressed. E-mail: cartier@ccr.jussieu.fr.
† Université Pierre et Marie Curie.
‡ Université Paris-Sud.

10.1021/jp049522h CCC: $27.50
Published on Web 07/27/2004

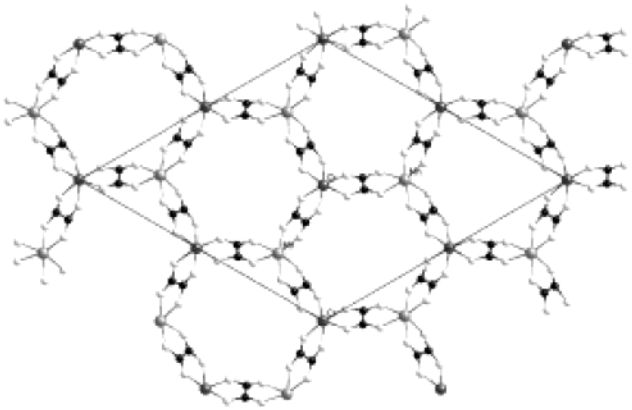

Figure 1. Honeycomb structure of a $[MnCr(ox)_3]^-$ 2D anionic layer in $TBA[MnCr(ox)_3]$ (adapted from ref 18).

oxalate-based magnets of general formula $\{A[M^{II}M^{III}(ox)_3]\}$, where A^+ is a monopositive cation.[17] In these compounds the anionic network $[M^{II}M^{III}(ox)_3]^-$ exhibits a honeycomb structure where the two metal ions occupy alternating crystallographic positions (Figure 1). The two metal ions are bischelated by three bridging oxalate ligands. Their environment is usually a trigonally distorted octahedron.[18,19]

In such an environment, the three cations are in their high spin state; for example, $S = {}^3/_2$ for Cr(III), $S = 2$ for Fe(II), and $S = {}^5/_2$ for Fe(III). The bridging oxalate ligands lead to an antiferromagnetic (AF) interaction between Fe(II) and Fe(III)[20] and a ferromagnetic (F) interaction between Fe(II) and Cr(III).[21] The synthesis and magnetic properties of the $\{[N(C_4H_9)_4][Fe^{II}Fe^{III}_xCr^{III}_{1-x}(ox)_3]\}$ series have been described in the literature.[14,15] In these compounds, there is a coexistence of the AF Fe(II)−Fe(III) and F Fe(II)−Cr(III) interactions. This leads to complex magnetic behaviors, including a possible spin-glass behavior,[14,15] and to a spectacular increase of the coercive force for x around 0.70.[15]

Synthesis. $K_3[Cr(ox)_3]\cdot 3H_2O$, $K_3[Fe(ox)_3]\cdot 3H_2O$, and $\{[N(C_4H_9)_4][Fe^{II}Fe^{III}_{0.77}Cr^{III}_{0.23}(ox)_3]\}$ were prepared according to the literature methods.[15,22] The other reagents are commercially available and were used as purchased. The Fe-to-Cr ratio in the compound is obtained through the ratio of the elemental analysis for Fe and Cr.

$\{[N(C_4H_9)_4][Fe^{II}Fe^{III}_{0.77}Cr^{III}_{0.23}(ox)_3]\}$. IR (KBr) cm^{-1} : 2970, s; 2940, m; 2879, m; 1623, vs; 1467, m; 1440, m; 1384, w; 1341, w; 1299, m; 912, w; 822, m; 546, m; 475, m; 432, m; 406, m. Anal. Calc for $C_{22}H_{36}NO_{12}Fe_{1.77}Cr_{0.23}$: C, 42.80; H, 5.88; N, 2.27; Fe, 16.01; Cr, 1.94. Found: C, 42.65; H, 6.15; N, 2.47; Fe, 15.22; Cr, 1.82.

Materials Analysis. The IR spectra were recorded on a Bio-Rad IRFT spectrophotometer as KBr pellets in the 4000−250 cm^{-1} region. Elemental analyses were completed at the SIARE-UPMC, Paris. Metal analyses were completed at Service Central d'Analyses, CNRS, Vernaison.

Magnetic Measurements. The magnetic measurements of powdered samples were performed between 2 and 300 K using a Quantum Design MPMS5 SQUID magnetometer. The hysteresis loops were measured at 2 and 14 K with a maximum field of 2 or/and 5 T. The field cooled (FC) magnetization versus temperature curves was measured in a 0.01 T external field. The susceptibility curve was measured in a 0.1 T external field.

XAS and XMCD Data Collection. The spectra were recorded at the Cr and Fe K-edges at the energy dispersive absorption line of the DCI ring at LURE (Orsay), using a Si(111) curved polychromator focusing the beam on the sample between the poles of a magnetic coil. Right circularly polarized photons were selected by positioning a 1 mm wide slit 5.5 mm below the "orbit plane", and the circular polarization rate was 70%. The recording temperature was $T = 14$ K, in the ferrimagnetic phase of the sample. In the electric dipolar approximation, reversing the magnetic field is equivalent to changing the helicity of the beam.[23] Hence, to record XMCD spectra, a first spectrum was registered with the magnetic field ($H = 2$ T) parallel to the propagation vector of the photons. Then, a second one was recorded with the magnetic field in the opposite direction. The XMCD signals were taken as the difference of the two spectra. The remnant XMCD signals were recorded at $H = 0$ T after applying alternatively the $H = 2$ T magnetic field parallel and antiparallel to the direction of the photon beam.

Results

Magnetic Properties. The χ^{-1} versus T curve is linear between 100 and 300 K. The magnetic susceptibility above 100 K closely obeys the Curie−Weiss law, $\chi = C/(T - \Theta)$. The Curie−Weiss temperature Θ deduced from the excellent fit of the χ^{-1} versus T curve between 100 and 300 K is −71 K. Below 100 K, χ^{-1} drops to much lower values when the temperature decreases. The zero field cooled (ZFC) and field cooled (FC) curves intersect at 36 K. This temperature thus corresponds to the critical temperature of the compound.

To compare the magnetic properties of the studied compound to those previously published by Coronado et al. on this series,[15] the hysteresis loop has been measured at 2 K (Table 1).

To correlate the macroscopic magnetic properties and the XMCD results, the hysteresis loop has been measured at 14 K, which is the temperature of the XMCD measurements (Table 1). To study the evolution of the magnetic properties with the temperature, the hysteresis loop was first measured up to 5 T. To establish a direct comparison with the XMCD results, the hysteresis loop was then measured with a maximum field of 2 T (Figure 2), which is the field used for the XMCD measurements. Under these conditions, the coercive field is 0.30 T, the magnetization $M_{\pm 2T}$ reaches 0.61 μ_b, and the remnant magnetization M_r is 0.18 μ_b. The $M_r/M_{\pm 2T}$ ratio is 0.30.

XANES and XMCD. The isotropic XANES, the XMCD signals (×1000), and the remnant XMCD signals (×1000) in zero field obtained at the iron and chromium K-edges are reported respectively in Figures 3 and 4.

K-edge XANES structures correspond to transitions of the 1s photoelectron to p-symmetry bound or continuum states according to the usual atomic selection rules in the electric

TABLE 1: Magnetic Data of the Studied Compound Extracted from the Hysteresis Loops Measured at 2 and 14 K[a]

	$T = 2$ K; $H_{max} = 5$ T			$T = 14$ K; $H_{max} = 5$ T			$T = 14$ K; $H_{max} = 2$ T		
x	$M_{\pm 5T}/\mu_b$	M_r/μ_b	H_c/T	$M_{\pm 5T}/\mu_b$	M_r/μ_b	H_c/T	$M_{\pm 2T}/\mu_b$	M_r/μ_b	H_c/T
0.75[15]	1.2	0.4	1.233						
0.77	1.01	0.25	1.03	1.05	0.21	0.36	0.61	0.18	0.30
0.80[15]	0.9	0.2	0.960						

[a] At 2 K, the data are compared to those previously published by Coronado et al.[15] for compounds with a close stoichiometry.

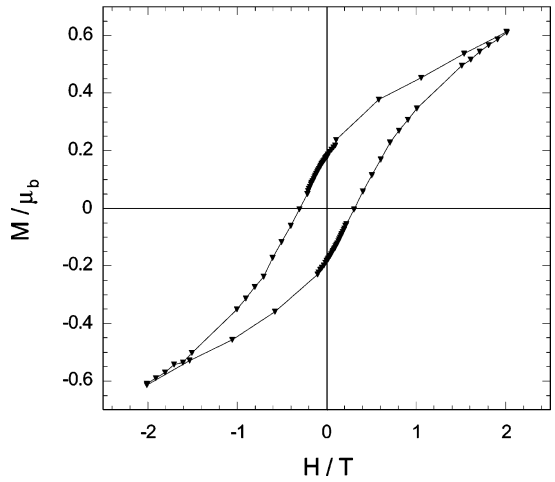

Figure 2. Hysterisis loop at 14 K with a maximum field of 2 T for $\{[N(C_4H_9)_4][Fe^{II}Fe^{III}_{0.77}Cr^{III}_{0.23}(ox)_3]\}$.

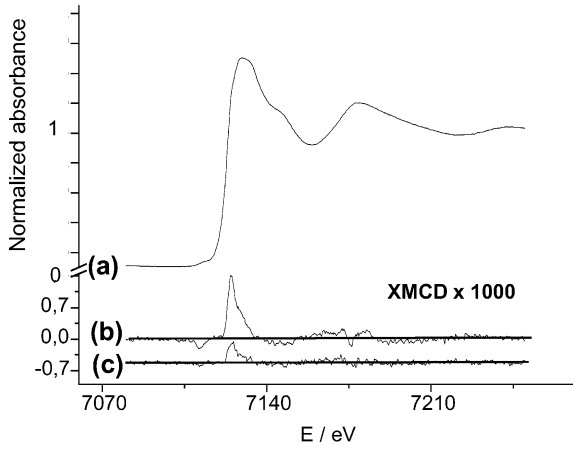

Figure 3. **(**a**)** Isotropic Fe K-edge XAS spectrum for $\{[N(C_4H_9)_4][Fe^{II}Fe^{III}_{0.77}Cr^{III}_{0.23}(ox)_3]\}$; **(**b**)** XMCD signals (×1000) measured in $H = \pm 2$ T; **(**c**)** XMCD signals (×1000) measured in zero field after applying $H = \pm 2$ T.

dipolar approximation. XANES spectra at the chromium K-edges display the main features expected for Cr(III) ions in nearly octahedral surroundings (Figure 4a).[13,24]

At the iron K-edge (Figure 3a), the two peaks at the absorption maximum are the signatures of the two oxidation states of the iron ions: Fe(II) at 7129 eV and Fe(III) at 7132 eV.[25]

A weak XMCD signal is present at the two edges (Figures 3b and 4b). The dichroic signal at the K-edges is due to the presence of spin−orbit coupling in the metallic 4p levels in the excited state ($1s^1 3d^n 4p^1$ electronic configuration) and the exchange interaction of the p excited electron with the 3d ones. The small intensity of the signals (0.14% of the isotropic spectrum for the iron ions and 0.08% for the chromium ions) is due to the absence of spin−orbit coupling in the 1s level and the weakness of the spin−orbit coupling in the final state.[26] The energy of the maximum of the signals corresponds, for both edges, to the beginning of the absorption jump (7125 eV for the iron and 6001 eV for the chromium). In iron mixed oxides, the XMCD signals coming from Fe(II) and Fe(III) ions are perfectly resolved and two distinct contributions separated by more than 3 eV are observed.[27] In our case, only one contribution is observed. Additional structures are observed around 40−50 eV after the absorption edges for both Cr and Fe K-edges. These features were predicted by multiple scattering calculations performed with potentials taking into account the spin−orbit

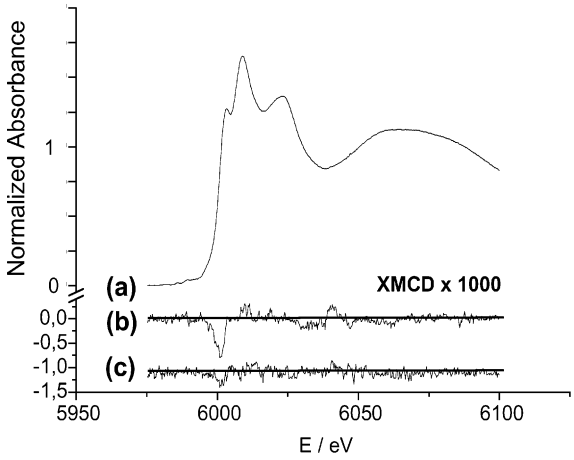

Figure 4. **(**a**)** Isotropic Cr K-edge XAS spectrum for $\{[N(C_4H_9)_4][Fe^{II}Fe^{III}_{0.77}Cr^{III}_{0.23}(ox)_3]\}$; **(**b**)** XMCD signals (×1000) measured in $H = \pm 2$ T; **(**c**)** XMCD signals (×1000) measured in zero field after applying $H = \pm 2$ T.

coupling which is responsible for XMCD.[28,29] For the iron K-edge, these features have also been qualitatively attributed to multiple excitations, but this proposition has never been demonstrated.[27]

After applying a magnetic field of $H = \pm 2$ T, a remnant signal is observed at the two edges when the magnetic field is switched off (Figures 3c and 4c). The shape is the same as that for XMCD spectra recorded with an ±2 T applied field. The intensity of the remnant signals is 0.043% of the isotropic signal at the Fe K-edge and 0.025% of the isotropic signal at the Cr K-edge. The ratio between the remnant and 2 T XMCD signals is 0.31 for both ions.

Discussion

Macroscopic Magnetic Properties. The magnetic properties measured for $\{[N(C_4H_9)_4][Fe^{II}Fe^{III}_{0.77}Cr^{III}_{0.23}(ox)_3]\}$ ($x = 0.77$) have to be compared to those published by Coronado et al. for 12 compounds in the $\{[N(C_4H_9)_4][Fe^{II}Fe^{III}_{x}Cr^{III}_{1-x}(ox)_3]\}$ series.[15]

Fitting the χ^{-1} versus T curve by a Curie−Weiss law corresponds to a mean field approach.[30] It thus gives access to the average interaction existing in the compound. The negative value of the Curie−Weiss constant obtained for $\{[N(C_4H_9)_4][Fe^{II}Fe^{III}_{0.77}Cr^{III}_{0.23}(ox)_3]\}$ confirms the predominance of the Fe(II)−Fe(III) antiferromagnetic interactions over the Fe(II)−Cr(III) ferromagnetic interactions for low Cr contents. Its critical temperature measured is just above the one obtained for $\{[N(C_4H_9)_4][Fe^{II}Fe^{III}_{0.80}Cr^{III}_{0.20}(ox)_3]\}$ (34.5 K).[15] The saturation and remnant magnetization values and the coercive force at 2 K fall between those found by Coronado et al. for $x = 0.75$ and $x = 0.80$ (Table 1). The magnetization at 2 K is far from being saturated with an applied magnetic field of 5 T.

Though the magnetic properties are far from being totally understood,[14,15] the studied compound fulfills the requirements imposed by our experimental setup for remnant XMCD measurements. The compound is definitely in its long-range ordered magnetic phase at 14 K. The coercive force remains strong enough to avoid relaxation problems. Moreover, the value of the $M_r/M_{\pm 2T}$ ratio at 14 K is high enough to obtain high quality reliable remnant XMCD signals despite the rather high temperature imposed by the experimental setup. To end, it is good to recall that metal ions with very different single ion anisotropies are present in the studied compound. This feature is important for theoretical reasons.[13]

Local Magnetic Properties. Let us turn now to the X-ray absorption measurements. At the iron K-edge, the XMCD signal under a ±2 T applied magnetic field appears at the beginning of the edge jump. Given its energy position, it shall mainly be attributed to Fe(II) species.

The sign of the dichroic signal is determined by the direction of the magnetic moments compared to the one of the magnetic field. The correspondence between the sign of the XMCD signal and the orientation of the magnetic moment is established thanks to measurements of the XMCD signals for model compounds. For the chromium ions, the shape of the XMCD signal, negative and then slightly positive, is the same as the one obtained for the molecule-based magnet $Cs^{I}Ni^{II}[Cr^{III}(CN)_6]$, in which the exchange interaction between Cr(III) and Ni(II) cations is ferromagnetic.[29] In our compound, the chromium local magnetic moments are thus parallel to the magnetic field. For the Fe ions, the signal first presents a very small negative part and then an important positive one. The sign is the opposite of the one obtained for a CoFe Prussian Blue analogue for which the local magnetic moment born by the iron ion was antiparallel to the magnetic field.[31] So here, the magnetic moments of Fe ions are parallel to the magnetic field. Due to the antiferromagnetic coupling between Fe(II) and Fe(III) ions, we expect that the Fe(II) which bears the majority spin is aligned parallel to the field while Fe(III) is aligned antiparallel. We thus expect that the XMCD signal is positive for the Fe(II) ion and negative for Fe(III). The positive sign of the resulting XMCD signal confirms that the iron XMCD signal mainly arises from Fe(II) species while Fe(III) is hardly seen.

Since the orientation of the magnetic moments of each species in the applied magnetic field can be directly deduced from the sign of the XMCD signals, this technique appears as a powerful tool for a direct and unambiguous determination of the nature of the exchange interaction in magnetic systems.[8,13,31] Due to the absence of an Fe(III) XMCD signal, we cannot determine the nature of the exchange interaction between Fe(II) and Fe(III). On the contrary, the existence of XMCD signals for Fe(II) and Cr(III) allows us to probe the interaction between those two metal ions despite the compound being macroscopically dominated by the AF Fe(II)−Fe(III) interaction in the paramagnetic phase. In the present case, the Fe(II) and Cr(III) magnetic moments are both parallel to the magnetic field applied, which indicates the ferromagnetic interaction between Fe(II) and Cr(III) ions in this compound. This corresponds to the interaction found through the sign of the Curie−Weiss constant in $\{[N(C_4H_9)_4][Fe^{II}Cr^{III}(ox)_3]\}$,[21] in agreement with a molecular interpretation of the exchange interaction in such systems.[1]

This technique appears as peculiarly attractive for compounds with exchange interactions of different nature and/or anisotropic ions. In such cases, the interpretation of the macroscopic magnetic measurements is rather complicated and sometimes misleading, as exemplified by Coronado et al. in the $[Fe^{II}Ru^{III}_x M^{III}_{1-x}(ox)_3]^-$ (M^{III} = Fe, Cr) series.[32,33]

Remnant Local Magnetization. XMCD and remnant XMCD signals at Fe (Figure 3b and c) and Cr (Figure 4b and c) K-edges can be compared to the macroscopic remnant magnetization measured at $T = 14$ K by conventional magnetometry (Figure 2). The ratio between the remnant XMCD signal and the XMCD signal obtained in a ±2T applied field is the same for both metal ions (0.31). This value is the same as the macroscopic magnetization ratio value obtained by SQUID measurement (0.30). Hence, the remnant to saturation XMCD signals ratios follow the macroscopic measurements for both ions: the local magnetic contribution of each ion to the total magnetization is the same with and without an applied magnetic field. According to the higher single ion anisotropy of the Fe(II) ion compared to the one of the Cr(III) ion, one would expect a higher remnant signal for the former ion compared to the latter. The similarity of the two signals indicates that, in this compound, the exchange interaction between the two metal ions is strong enough to transfer the single ion anisotropy of one cation to the other, for example, to wipe out the intrinsic difference between the single ion anisotropies. As exemplified in experimental[12] and theoretical[10] works undertaken on single molecule magnets as well as in extended networks,[32] this result underlines the complex relationship between the single ion anisotropies and the hysteretic behavior.

Measurements at the metal ions' $L_{2,3}$-edges are planned for this system. First, the separation of the Fe(II) and Fe(III) contributions will be more obvious given the better resolution expected.[34] We will thus gain insight into the magnetic behavior of the Fe(III) ion by determining the possible existence of a net magnetic moment and its orientation in the field. The nature of the exchange interaction with the other metal ions will then be more clearly established. Moreover, such measurements would allow us to quantify the role of single ion anisotropy in the remnant magnetic behavior through the determination of the orbital contribution to the magnetic moment of each spin carrier thanks to multiplet calculations.[9] In the present system, the orbital moment of the Fe(II) ion, and hence its anisotropy, is expected to be much higher than those for the Fe(III) ($3d^5$) and Cr(III) ($3d^3$) ions.

We have performed experiments at $L_{2,3}$-edges on such systems using the total yield electron detection mode. Due to the small probing depth (few tens of angstroms) of this detection mode,[35] we did not observe any remnant XMCD signal despite the existence of a macroscopic remnant magnetization. This shows that there is no surface hysteretic behavior. Experiments shall be undertaken using the fluorescence detection mode, whose probing depth is much larger.[36] Such a detector is at the time being tested on our experimental setup.

Summary

We report XMCD results at the Fe and Cr K-edges for the oxalate-based magnet $\{[N(C_4H_9)_4][Fe^{II}Fe^{III}_{0.77}Cr^{III}_{0.23}(ox)_3]\}$. The analysis of macroscopic and XMCD magnetic measurements supports the proposed spin-glass behavior of this compound[14,15] and relates it to Fe(III) ions. The Fe(II)−Cr(III) ferromagnetic exchange interaction is directly evidenced though, in the paramagnetic phase, the negative value of the Curie−Weiss temperature indicates that it is macroscopically dominated by the antiferromagnetic Fe(II)−Fe(III) interaction. We evidenced a remnant XMCD signal at $H = 0$ T at the two edges. We show that the contribution of the local magnetic moments to the total remnant magnetization is the same for Cr(III) and Fe(II) cations despite the higher single ion anisotropy of the Fe(II) ion. This result is in line with other XMCD investigations on the origin of the hysteretic behavior of single molecule magnets[10,12] and of extended networks.[13]

These experiments in zero field open new perspectives. They can be used to suppress undesirable signals arising from paramagnetic impurities in the studied compounds.[12] Moreover, a remnant XMCD signal of a paramagnetic ion included in a magnetically long-range-ordered material would arise from the internal magnetic field created by the magnetic network. This new probe of the internal magnetic field, compared to Mössbauer spectroscopy,[37] would not be restricted to iron containing compounds.

Acknowledgment. The authors thank CNRS (France), Université "Pierre et Marie Curie" (France), European community (TMR ERBFMBICT972644 and FMRXCT980181), and European Science Foundation (Molecular Magnets Programme) for financial support. The authors are grateful to Dr. Christine Giorgetti for technical support during the XMCD measurement. They address special thanks to Dr. Anne Bleuzen for fruitful scientific discussions.

Supporting Information Available: Figures showing the temperature dependence of χ^{-1} together with the Curie−Weiss fit between 100 and 300 K and the zero field cooled/field cooled curves. This material is available free of charge via the Internet at http://pubs.acs.org.

References and Notes

(1) Kahn, O. *Molecular Magnetism*; VCH: Weinhem, 1993.
(2) *Magnetism: Molecules to Materials I−III*; Wiley-VCH: Weinheim, 2001−2002.
(3) Sessoli, R.; Gatteschi, D.; Caneschi, A.; Novak, M. *Nature* **1993**, *365*, 141.
(4) Sessoli, R.; Tsai, H.-L.; Schake, A.; Wang, S.; Vincent, J.; Folting, K.; Gatteschi, D.; Christou, G.; Hendrickson, D. *J. Am. Chem. Soc.* **1993**, *115*, 1804.
(5) Gatteschi, D. *Philos. Trans. R. Soc. London, A* **1999**, *357*, 3079.
(6) Rudolf, P.; Sette, F.; Tjeng, L. H.; Meigs, G.; Chen, C. T. *J. Magn. Magn. Mater.* **1992**, *109*, 109.
(7) Ebert, H.; Schütz, G. *Spin−Orbit Influenced Spectroscopies of Magnetic Solids; Lecture notes in Physics*; Springer-Verlag: Berlin, 1996.
(8) Dujardin, E.; Ferlay, S.; Phan, X.; Desplanches, C.; Cartier dit Moulin, C.; Sainctavit, P.; Baudelet, F.; Dartyge, E.; Veillet, P.; Verdaguer, M. *J. Am. Chem. Soc.* **1998**, *120*, 11347.
(9) Carra, P.; Thole, T.; Altarelli, M.; Wang, X. *Phys. Rev. Lett.* **1993**, *70*, 694.
(10) Moroni, R.; Cartier dit Moulin, C.; Champion, G.; Arrio, M. A.; Sainctavit, P.; Verdaguer, M.; Gatteschi, D. *Phys. Rev. B* **2003**, *68*, 064407/1.
(11) Sangregorio, C.; Ohm, T.; Paulsen, C.; Sessoli, R.; Gatteschi, D. *Phys. Rev. Lett.* **1997**, *78*, 4645.
(12) Letard, I.; Sainctavit, P.; Gatteschi, D.; Cartier dit Moulin, C.; Champion, G.; Kappler, J. P. *Phys. Scr.*, to be published.
(13) Train, C.; Giorgetti, C.; Baudelet, F.; Champion, G.; Cartier dit Moulin, C. *C. R. Chim.* **2003**, *6*, 337.
(14) Bhattacharjee, A.; Iijima, S.; Mizutani, F. *J. Magn. Magn. Mater.* **1996**, *153*, 235.
(15) Coronado, E.; Galan-Mascaros, J. R.; Gomez-Garcia, C. J.; Martinez-Agudo, J. M. *Adv. Mater. (Weinheim, Ger.)* **1999**, *11*, 558.
(16) Weltner, W. *Magnetic atoms and molecules*; Dover Publications: New York, 1983; p 256.
(17) Clément, R.; Decurtins, S.; Gruselle, M.; Train, C. *Monatsh. Chem.* **2002**, 497.
(18) Decurtins, S.; Schmalle, H. W.; Oswald, H. R.; Linden, A.; Ensling, J.; Guetlich, P.; Hauser, A. *Inorg. Chim. Acta* **1994**, *216*, 65.
(19) Atovmyan, L. O.; Shilov, G. V.; Lyubovskaya, R. N.; Zhilyaeva, E. I.; Ovanessyan, N. S.; Bogdanova, O. A.; Perumova, S. I. *Russ. J. Coord. Chem.* **1997**, *23*, 683.
(20) Mathonière, C.; Nuttall, C. J.; Carling, S. G.; Day, P. *Inorg. Chem.* **1996**, *35*, 1201.
(21) Tamaki, H.; Zhong, Z. J.; Matsumoto, N.; Kida, S.; Koikawa, M.; Achiwa, N.; Hashimoto, Y.; Okawa, H. *J. Am. Chem. Soc.* **1992**, *114*, 6974.
(22) Bailar, J. C.; Jones, E. M. *Inorg. Synth.* **1939**, *1*, 35.
(23) Born, M.; Wolf, E. *Principle of optics*; Pergamon Press: London, 1959.
(24) Verdaguer, M.; Mallah, T.; Helary, C.; L'Hermite, F.; Sainctavit, P.; Arrio, M.-A.; Babel, D.; Baudelet, F.; Dartyge, E.; Fontaine, A. *Physica B* **1995**, *208−209*, 765.
(25) Scarrow, R. C.; Trimitsis, M. G.; Buck, C. P.; Grove, G. N.; Cowling, R. A.; Nelson, M. J. *Biochemistry* **1994**, *33*, 15023.
(26) Carra, P.; König, H.; Thole, T.; Altarelli, M. *Physica B* **1993**, *192*, 182.
(27) Dartyge, E.; Baudelet, F.; Brouder, C.; Fontaine, A.; Giorgetti, C.; Kappler, J. P.; Krill, G.; Lopez, M. F.; Pizzini, S. *Physica B* **1995**, *208 & 209*, 751.
(28) Brouder, C.; Alouani, M.; Bennemann, K. *Phys. Rev. B* **1996**, *54*, 7334.
(29) Sainctavit, P.; Cartier dit Moulin, C.; Arrio, M.-A. In *Magnetism: Molecules to Materials*; Miller, J., Drillon, M., Eds.; Wiley-VCH: Weinheim, 2001; p 142.
(30) Herpin, A. *Théorie du Magnétisme*; Presses Universitaires de France: Paris, 1968.
(31) Champion, G.; Escax, V.; Cartier dit Moulin, C.; Bleuzen, A.; Villain, F.; Baudelet, F.; Dartyge, E.; Verdaguer, M. *J. Am. Chem. Soc.* **2001**, *123*, 12544.
(32) Coronado, E.; Galan-Mascaros, J. R.; Gomez-Garcia, C. J.; Martinez-Agudo, J. M. *Synth. Met.* **2001**, *122*, 501.
(33) Larianova, J.; Mombelli, B.; Sanchiz, J.; Kahn, O. *Inorg. Chem.* **1998**, *37*, 679.
(34) Cartier dit Moulin, C. Interaction of X-rays with matter. In *Magnetism and Synchrotron Radiation*; Beaurepaire, E., Carrière, B., Kappler, J. P., Eds.; Les Editions de Physique: Les Ulis, 1997; p 16.
(35) Abbate, M.; Goedkoop, J. B.; de Groot, F. M. F.; Grioni, M.; Fuggle, J. C.; Hofmann, S.; Petersen, H.; Sacchi, M. *Surf. Interface Anal.* **1992**, *18*, 65.
(36) Nemanova, V. I.; Kondratenko, A. V.; Ruzankin, S. F.; Bausk, N. V.; Zhidomirov, G. M.; Mazalov, L. N. *Chem. Phys.* **1987**, *116*, 61.
(37) Coronado, E.; Galan-Mascaros, J. R.; Gomez-Garcia, C. J.; Martinez-Agudo, J. M.; Martinez-Ferrero, E.; Waerenborgh, J. C.; Almeida, M. *J. Solid State Chem.* **2001**, *159*, 391.